IJC
International Journal of Cancer

Extracellular vesicles from human liver stem cells inhibit renal cancer stem cell-derived tumor growth *in vitro* and *in vivo*

Alessia Brossa[1,2], Valentina Fonsato[2,3], Cristina Grange[4], Stefania Tritta[2], Marta Tapparo[4], Ruggero Calvetti[1], Massimo Cedrino[2], Sofia Fallo[1], Paolo Gontero[5], Giovanni Camussi[4] and Benedetta Bussolati[1,2]

[1]Department of Molecular Biotechnology and Health Sciences, University of Torino, Torino, Italy
[2]Molecular Biotechnology Center, University of Torino, Torino, Italy
[3]2i3T, Società per la Gestione dell'incubatore di Imprese e per il Trasferimento Tecnologico, University of Torino, Torino, Italy
[4]Department of Medical Science, University of Torino, Torino, Italy
[5]Department of Surgical Sciences, University of Torino, Torino, Italy

Cancer stem cells (CSCs) are considered as responsible for initiation, maintenance and recurrence of solid tumors, thus representing the key for tumor eradication. The antitumor activity of extracellular vesicles (EVs) derived from different stem cell sources has been investigated with conflicting results. In our study, we evaluated, both *in vitro* and *in vivo*, the effect of EVs derived from human bone marrow mesenchymal stromal cells (MSCs) and from a population of human liver stem cells (HLSCs) of mesenchymal origin on renal CSCs. *In vitro*, both EV sources displayed pro-apoptotic, anti-proliferative and anti-invasive effects on renal CSCs, but not on differentiated tumor cells. Pre-treatment of renal CSCs with EVs, before subcutaneous injection in SCID mice, delayed tumor onset. We subsequently investigated the *in vivo* effect of MSC- and HLSC-EVs systemic administration on progression of CSC-generated renal tumors. Tumor bio-distribution analysis identified intravenous treatment as best route of administration. HLSC-EVs, but not MSC-EVs, significantly impaired subcutaneous tumor growth by reducing tumor vascularization and inducing tumor cell apoptosis. Moreover, intravenous treatment with HLSC-EVs improved metastasis-free survival. In EV treated tumor explants, we observed both the transfer and the induction of miR-145 and of miR-200 family members. In transfected CSCs, the same miRNAs affected cell growth, invasion and survival. In conclusion, our results showed a specific antitumor effect of HLSC-EVs on CSC-derived renal tumors *in vivo*, possibly ascribed to the transfer and induction of specific antitumor miRNAs. Our study provides further evidence for a possible clinical application of stem cell-EVs in tumor treatment.

Introduction

Renal cell carcinoma (RCC) is a common solid tumor, the third among urogenital malignancies, and appears one of the fastest increasing cancers in the last 10 years.[1] RCC is often associated with high recurrence with frequent metastatic spread, leading to high mortality.[2] In addition, RCC is resistant to common chemotherapeutic drugs, while the response to tyrosine kinase inhibitors is impaired within time by the selection of a resistant population.[3] Indeed, cancer stem cells (CSCs) are now considered the responsible for the initiation, maintenance and recurrence of solid tumors.[4] In RCC, a CSC population with stem-like properties has been identified by several groups,[5] by expression of different functional and surface markers, including endoglin (CD105).[6] In addition, renal CSCs express mesenchymal markers, such as CD44, CD90, CD146, CD73, CD29, vimentin and embryonic stem cells markers such as Nanog, Oct4, Musashi, Nestin and Pax2 whereas they lack the expression of epithelial differentiation markers.[6]

Targeting of renal CSCs represents an important approach to eradicate RCC, considering their high drug resistance and tumor-initiating capability. Extracellular vesicles (EVs) play a key role in cell communication by transferring mRNAs, microRNAs (miRNAs), lipids and proteins to target cells.[7–9] In particular, stem cell-derived EVs are known to reprogram target cells and promote tissue repair by transferring their

A.B. and V.F. contributed equally to this work

Additional Supporting Information may be found in the online version of this article.

Key words: renal cell carcinoma, exosomes, microRNA, exRNA, antitumor therapy

DOI: 10.1002/ijc.32925

History: Received 19 Jul 2019; Accepted 4 Feb 2020; Online 13 Feb 2020

Correspondence to: Benedetta Bussolati, E-mail: benedetta.bussolati@unito.it

What's new?

Stem cell-derived extracellular vesicles (EVs) can reprogram target cells and promote tissue repair by transferring their cargo. However, the anti-tumor activity of EVs derived from different stem cell sources has been investigated with conflicting results. Here, the authors demonstrate for the first time the anti-tumor effect of EVs from human liver stem cells (HLSC-EVs) in a systemic intravenous administration model. HLSC-EVs had a selective effect on cancer stem cells that could be ascribed to the transfer and induction of anti-tumor miRNAs. This study highlights the potential clinical use of stem cell-derived EVs, alone or in combination with other cancer therapies.

cargo.[9] However, their role in tumor development has been controversial. In particular, mesenchymal stromal cells (MSCs) derived EVs may display pro and antitumor effects.[10] Recently, EVs derived from human liver stem cells (HLSCs), another source of human resident mesenchymal stromal cells isolated from the liver, showed an anti-angiogenic effect on renal tumor-derived endothelial cells, both *in vitro* and *in vivo*.[11] Interestingly, MSC-EVs did not share the *in vitro* and *in vivo* anti-angiogenic effect of HLSC-EVs, possibly due to a specific miRNA signature,[12] including differential expression of anti-angiogenic miRNAs (miR-15a, miR-181b, miR-320c and miR-874).[11] Moreover, HLSC-EVs induced *in vitro* apoptosis of renal CSCs, alone and in synergy with tyrosine kinase inhibitors.[13] However, no studies at present evaluated the effect of stem cell-derived EVs on RCC and/or renal CSCs *in vivo*. In our study, we aimed to dissect the effect of a systemic HLSC-EV treatment *in vivo* on renal CSC-induced tumors, and we correlated their antitumor activity with EV cargo.

Materials and Methods

Renal CSCs and RCC isolation and culture

Renal CSCs and RCC were isolated and characterized as previously described.[6,14] Briefly, cells were obtained from specimens of renal cell carcinomas from patients undergoing radical nephrectomy according to the Ethics Committee of the S. Giovanni Battista Hospital of Torino, Italy (168/2014). CSCs were isolated from the total RCC population, using anti-CD105 Ab by magnetic-activated cell sorting (MACS) system (Miltenyi Biotec, Auburn, CA). CD105 positive CSCs were cultured in the presence of the expansion medium, consisting of DMEM LG (Invitrogen, Carlsbad, CA), with insulin–transferrin–selenium, 10^{-9} M dexamethasone, 100 U penicillin, 1,000 U streptomycin, 10 ng/ml EGF (all from Sigma-Aldrich, St. Louis, MO) and 5% fetal calf serum (FCS; Euroclone, MI, Italy). For cell cloning, single cells were seeded in 96-well plates in the presence of the expansion medium. A G7 and a D2 CD105 positive clonal renal cell carcinoma stem cell line was selected and used for all the experiments. Total RCC population was maintained in culture in DMEM LG (Invitrogen), and 10% fetal calf serum (FCS) (Euroclone). Mycoplasma absence in primary cells in the study was routinely tested using RT-PCR.

HLSCs and MSCs culture

HLSCs were isolated from human cryopreserved normal hepatocytes obtained from Lonza (Basel, Switzerland), characterized and cultured as previously described.[15–18] Human hepatocytes were plated in the presence of alfa minimum essential medium/endothelial cell basal medium (expansion media: α-MEM/EBM in the ratio 3:1, Lonza), supplemented with antibiotics (100 U penicillin and 1,000 U streptomycin; both from Sigma-Aldrich) and 10% Fetal Calf Serum (FCS, Euroclone). After 2 weeks, HLSC colonies were expanded. HLSC expressed several mesenchymal markers and, at variance with oval liver cells, did not express c-kit, CD34 and cytokeratin 19 and showed multiple differentiative abilities.[15] MSCs, that represent a mesoderm derived population of progenitors, were obtained from Lonza and cultured and characterized as previously described.[19] MSCs were used up to the sixth passage of culture. Mycoplasma absence in primary cells in the study was routinely tested using RT-PCR.

EVs isolation and characterization

The supernatant of HLSCs or MSCs, cultured overnight in serum-free media, was recovered and centrifuged for 20 min at 3,000*g* and submitted to microfiltration (0.22 μm filter, Merck-Millipore, Burlington, MA) to remove cell debris and apoptotic bodies. Then, supernatants were submitted to ultracentrifugation at 100,000 g for 2 hr at 4°C (Beckman Coulter Optima L-90K, Fullerton, CA). Both HLSC-EVs and MSC-EVs were resuspended in RPMI supplemented with 1% dimethyl sulfoxide (DMSO, Sigma-Aldrich) and stored at −80°C for later use. Concentration and size distribution of EVs were determined by the Nanosight LS300 system (Malvern Panalytical, Malvern, UK). Briefly, EV preparations were diluted (1:200) in sterile saline solution and analyzed by the Nanoparticle Analysis System using the NTA 1.4 Analytical Software (Supporting Information Fig. S1*a*).[13] EV purity was assessed as ratio of *n*. EV/microgram protein.[20] Electronic microscopy was performed as previously described.[12] Moreover, HLSC-EVs were characterized by Guava analysis (Merck-Millipore) for the expression of exosomal markers CD63 and CD81 and the markers of cells of origin CD44 and CD29 (all from Beckton Dickinson, Franklin Lakes, NJ; Supporting Information Fig. S1*b*). FITC and PE mouse non-immune Isotypic IgG (Beckton Dickinson) served as controls. EVs were incubated with each antibody, or isotype control

antibody at 4°C in 100 µl PBS (Lonza) containing 0.1% bovine serum albumin, and analyzed. All samples were gated on the basis of negative controls and compensated appropriately prior to analyses. The characteristics of HLSC-EVs are similar to those described for EVs derived by MSC.[21] For biodistribution experiments, MSC-EVs and HLSC-EVs were labeled during ultracentrifugation with 1 µM Vybrant Cell Tracers DiD fluorescent dye (TermoFisher Scientific, Waltham, MA) as previously described.[19] Labeled EVs were therefore washed twice by ultracentrifugation in PBS (Lonza).

Proliferation

For proliferation assay, cells were plated at a concentration of 1,500 renal CSCs/well, in a 96-multiwell plate and cultured with different doses of HLSC-EVs or MSC-EVs (5, 10 or 50×10^3 EV/target cell). DNA synthesis was detected after 48 hr as incorporation of 5-bromo-2-deoxyuridine (BrdU) using an enzyme-linked assay kit (Chemicon, Fisher Scientific, Hampton, NH). Data are expressed as the mean ± SD of the mean of absorbance of at least three different experiments, normalized to control (not treated cells).

Apoptosis

Cytofluorimetric evaluation of apoptotic cells was performed using the Muse™ Annexin V & Dead Cell Kit (Merck-Millipore), according to the manufacturer's recommendations. Briefly, 25×10^3 cells were incubated with 50×10^3 HLSC-EVs/target cells for 48 hr. Cells were then detached and resuspended in Muse™ Annexin V & Dead Cell Kit, and the percentage of apoptotic cells (Annexin V +) was detected. The assay utilizes Annexin V to detect phosphatidylserine on the external membrane of apoptotic cells. A dead cell marker (7-AAD) is also used as an indicator of cell membrane structural integrity.

Invasion

Invasion was evaluated in 24-well cell culture inserts (Beckton Dickinson) with a porous membrane (8.0 µm pore size) precoated with 100 µg Matrigel per well as previously described.[22] Briefly, 50×10^3 renal CSCs were plated in the presence of 5, 10 or 50×10^3 HLSC-EVs or MSC-EVs/target cell in the upper side of the precoated transwell in DMEM (Euroclone). As attractive stimulus, complete culture medium was added in the well. After 48 hr, cells that moved from the upper side to the lower one of the transwell were fixed in MetOH and stained with crystal violet (Sigma-Aldrich). Total area of invaded Matrigel (magnification: 100×) was evaluated by ImageJ at least five pictures per transwell.

Sphere formation

To grow renal CSCs in nonadhesive condition as floating spheres, cells were plated at 1×10^5 cells/ml in serum-free DMEM-F12 (Cambrex BioScience, Charles City, IA), supplemented with 10 ng/ml bFGF, 20 ng/ml EGF, 5 µg/ml insulin and 0.4% bovine serum albumin (all from Sigma-Aldrich), as described,[5,13,14] in the presence of 10 or 50×10^3 HLSC-EVs or MSC-EVs/target cell for 72 hr. Sphere viability was then measured by MTT (3-(4,5-dimetiltiazol-2-yl)-2,5-difeniltetrasodium bromide, Merck-Millipore), as previously described.[23] Briefly, spheroids were centrifuged and resuspended in 300 µl of PBS solution for efficient disaggregation. Spheroid-derived cells were then plated in 96-well plates in triplicates and analyzed according to manufacturer's instructions. Data are expressed as mean ± SD of the mean absorbance of three different experiments performed in triplicates and normalized to untreated cells.

In vivo subcutaneous model of CSC-derived renal tumor

All animal studies were conducted in accordance with the national guidelines and regulations and were approved by the Ethics Committee of the University of Torino (Protocol Number: 338/2016-PR). In order to evaluate the effect of HLSC-EVs on renal CSCs tumor growth, renal CSCs were implanted subcutaneously into SCID mice (Charles River, Wilmington, MA) within growth factor-reduced Matrigel (Beckton Dickinson). Briefly, 1×10^3 renal CSCs were resuspended in 75 µl DMEM plus 125 µl of Matrigel at 4°C and immediately injected subcutaneously SCID mice. Two plugs/mouse was performed. In pretreatment experiments, cells were treated with 50×10^3 HLSC-EVs or MSC-EVs/target cell for 24 hr prior to cell injection. In treatment experiments, mice were treated intravenously with HLSC-EVs (1×10^{10} EVs/mouse/injection) or PBS twice per week for 4 weeks, starting 1 week after cell injection. Tumors were measured with a caliper once per week. Five weeks after cell injection, mice were sacrificed, plugs recovered and processed for histological and molecular analysis. Isolation of $CD105^+$ CSCs from plugs was performed using the magnetic-activated cell sorting (MACS) system (Miltenyi Biotec, Auburn, CA).

Tunel assay (ApopTag Apoptosis Detection Kit; Merck Millipore) was performed on paraffin-embedded sections in order to evaluate renal tumor cell apoptosis in recovered plugs, following the manufacturer's instructions. The amount of apoptotic cells was evaluated by counting the number of Tunel positive cells per field in 10 randomly chosen fields per tumor section (magnification: 400×) using ImageJ software.

Optical imaging and biodistribution of EVs

SCID mice were subcutaneously with 1×10^3 renal CSCs within Matrigel. After 3 weeks, mice were treated with 1.5×10^{10} labeled EVs/mouse (MSC- and HLSC-EVs), using two different routes of EV administration to compare tumor EV localization. Mice were sacrificed at different time points (5, 24 and 48 hr post-EV administration) and dissected tumors were subjected to Optical Imaging ($n = 3$ per EV type, administration route and time point). All studies were performed with IVIS 200 small animal imaging system (PerkinElmer, Waltham, MA) using excitation filter at

640 nm and an emission filter at 700 nm. Fluorescence emission was normalized to photons per second per centimeter squared per steradian (p/sec/cm^2/sr) as previously described.[19] The fluorescence signal was quantified in tumors in ROI draw freehand. The relative mean fluorescence intensity of each ROI was obtained by subtracting the mean fluorescence intensity of the corresponding ROI of the fluorescence intensity of mice not treated with labeled EVs. Data were expressed as the average radiance ± SD. Images were acquired and analyzed using Living Image 4.0 software (Perkin Elmer).

Generation of luciferase-expressing CSCs (LUC-CSCs)

Renal CSCs were infected with a lentivirus containing the pBMN(CMV-copGFP-Luc2-Puro) plasmid (Addgene plasmid # 80389).[24] Briefly, 293T cells were transfected with constructs using ViraPower Packaging Mix (Life Technologies, Carlsbad, CA) for lentiviruses production, according to manufacturer's instructions. After titering the lentiviral stock, renal CSCs were infected with lentiviral particles following the manufacturer's instructions. Cells were selected by puromycin (Gibco, Thermofisher; 1 μg/ml) and, after 1 week, antibiotic-resistant cells were expanded. Cell infection was considered effective when the percentage of GFP positive cells was >95%, as assessed by cytofluorimetric analysis (data not shown). Firefly luciferase expression on renal CSCs was assessed by IVIS 200 small animal imaging system (PerkinElmer) by incubating 20 μg D-Luciferin (PerkinElmer) in 100 μl complete medium containing different cell numbers (1×10^2–1×10^6). Cells were considered effectively expressing luciferase when the signal of 1×10^3 cells was detected (data not shown).

Hematogenous CSCs spread to the lungs

Hematogenous CSCs spread to the lungs was induced in SCID mice (Charles River) by injecting 5×10^5 LUC-CSCs in the tail vein. One week after cell injection, mice were treated intravenously with HLSC-EVs or PBS twice per week for 4 weeks. The formation of lung tumor colonies was monitored weekly with IVIS 200 small animal imaging system (PerkinElmer). Images were acquired whole body and analyzed using Living Image 4.0 software (PerkinElmer).[25] Briefly, mice were anesthetized by isoflurane inhalation and then injected intraperitoneally with 3 mg D-luciferin (PerkinElmer). Ten minutes after injection, bioluminescent data were collected with an imaging time of 3 min.

The luminescence was quantified in the region of interest (ROI) draw freehand. A mouse was considered positive for lung tumor formation when luminescence values were at least 3.5 times higher than mice not bearing lung tumor foci. Data were expressed as average radiance ± SD.

mRNA and miRNA isolation and real-time PCR

Total RNA was isolated from different preparations using Trizol Reagent (Ambion, Thermofisher) according to the manufacturer's protocol. RNA was then quantified spectrophotometrically (Nanodrop ND-1000, Thermofisher). For gene expression analysis, quantitative Real-time PCR was performed. Briefly, first-strand cDNA was produced from 200 ng total RNA using the High Capacity cDNA Reverse Transcription Kit (Applied Biosystems, Foster City, CA) or, for miRNA analysis, the miScript Reverse Transcription Kit (Qiagen, Hilden, Germany). Real-time PCR experiments were performed in 20 μl reaction mixture containing 5 ng of cDNA template, the sequence-specific oligonucleotide primers (purchased from MWG-Biotech, Nantes, BRU, Luxembourg) and the Power SYBR Green PCR Master Mix (Applied Biosystems), or miScript SYBR Green PCR Kit (Qiagen). TBP mRNA, or RNU48 were used to normalize mRNA or miRNA inputs, respectively. The sequence-specific oligonucleotide used for mRNA analysis is TBP Fw: 5′-TGT GCA CAG GAG CCA AGA GT-3′; Rev: 5′-ATT TTC TTG CTG CCA GTC TGG-3′; C-MYC Fw: 5′-CAG CGA CTC TGA GGA GGA ACA-3′; Rev: 5′-TGA GGA GGT TTG CTG TGG C-3′; EGFR Fw: 5′-GTG ACC GTT TGG GAG TTG ATG A-3′; Rev: 5′-GGC TGA GGG AGG CGT TCT C-3′; ZEB1 Fw: 5′-GAA GAG ATC AAA GAC ATG TGA CGC-3′; Rev: 5′-TCT CCA CTG TGA ATT CTT AAG TGC TC-3′; ZEB2 Fw: 5′-CCA CGA TCC AGA CCG CA-3′; Rev: 5′-GTA CTC CTC GAT GTC GAC TGC A-3′; MMP1 Fw: 5′-CCA ACA ATT TCA GAG AGT ACA ACT TAC AT-3′; Rev: 5′-TGA AGG TGT AGC TAG GGT ACA TCA AA-3′. The Fw sequence-specific oligonucleotide used for miRNA analysis are hsa-miR-24-3p: 5′-TGG CTC AGT TCA GCA GGA A-3′; hsa-miR-29a-3p: 5′-TAG CAC CAT CTG AAA TCG GTT-3′; hsa-miR-31-5p: 5′-AGG CAA GAT CCT GGC ATA G-3′; hsa-miR-Let7b-5p: 5′-TGA GGT AGT AGG TTG TGT GGT T-3′; hsa-miR-141-3p: 5′-TAA CAC TGT CTG GTA AAG ATG G-3′; hsa-miR-145-5p: 5′-GTC CAG TTT TCC CAG GAA TCC-3′; hsa-miR-200a-3p: 5′-TAA CAC TGT CTG GTA ACG ATG T-3′; hsa-miR-200b-3p: 5′-TAA TAC TGC CTG GTA ATG ATG A-3′; hsa-miR-200c-3p: 5′-ACT GCC GGG TAA TGA TGG A-3′; hsa-miR-223-3p: 5′-TGT CAG TTT GTC AAA TAC CCC A-3′; hsa-miR-429: 5′-TAA TAC TGT CTG GTA AAA CCG T-3′; hsa-miR-451a: 5′-AAA CCG TTA CCA TTA CTG AGT T-3′; RNU-48: 5′-AAC TCT GAG TGT GTC GCT GAT G-3′.

Cell transfection

Transfection of renal CSCs was performed using HiPerfect reagent (Qiagen) as previously described.[12] Briefly, 1×10^5 renal CSCs/well were plated in a 12-well plate and left adhere overnight. The day after, medium was replaced with 1 ml DMEM containing 10 μl HiPerfect reagent (Qiagen) and 100 pmol of the specific mimic miRNAs (all from Qiagen). The day after transfection fresh growth medium was replaced and on Day 2, the cells were used for *in vitro* experiments (proliferation, apoptosis and invasion assay) or gene expression analysis (Real-time PCR). Cells transfected with scramble mimic (Qiagen) were used as control.

Transcription inhibition with α-Amanitin

Renal CSCs were seeded in six-well plate (2×10^5/well) and left to adhere overnight. The next day, cells were incubated with the transcriptional inhibitor, α-Amanitin (50 μg/ml, Sigma-Aldrich, St. Louis, MO) either in the absence or in the presence of 5×10^4 HLSC-EVs/target cell. Cells were collected for RNA extraction and real-time PCR analysis 1, 3 or 6 hr after.

Statistical analysis

Statistical analysis was performed by using the Student *t*-test or ANOVA with Dunnet's multicomparison tests, as appropriate. A value of $p < 0.05$ was considered significant. All statistical analyses were carried out on Graph Pad Prism version 5.04 (Graph Pad Software, Inc, La Jolla, CA).

Data availability

The experimental data that support the findings of our study are available from the corresponding author upon reasonable request.

Results

Stem cell-derived EVs reduce proliferation, sphere formation and invasion of renal CSCs

We recently showed that EVs from HLSCs induced renal CSCs apoptosis.[13] In order to extend the effect of HLSC-EVs to *in vivo* treatment, we first tested their effect on proliferation, sphere formation and invasion ability of two different renal CSC lines, and compared their effect with that of bone marrow-derived MSC-EVs, a mesoderm derived population of progenitors. Stem cell-derived EVs were isolated by ultracentrifugation and characterized as previously described.[11,13] Similar size and distribution of MSC- and HLSC-EVs were assessed by NanoSight analysis and by electron microscopy (Supporting Information Fig. S1*a*). Moreover, by cytofluorimetric Guava analysis, we found that both sources expressed markers of exosomes and of the originating cells (CD81, CD63 and CD29, CD105, CD73 respectively), while the hematopoietic marker CD45 was not detectable (Supporting Information Fig. S1*b*). As reported,[13] HLSC-EVs, but not MSC-EVs, displayed a proapoptotic effect on renal CSCs (Supporting Information Fig. S1*c*). Moreover, EVs from both stem cell sources impaired proliferation of renal CSCs obtained from two different RCC samples in a dose-dependent manner (Fig. 1*a*). In addition, they significantly reduced the capability of renal CSCs to form spheres, a characteristic ability of CSCs (Fig. 1*b*) and significantly limited their invasion ability (Figs. 1*c* and 1*d*).

To evaluate the possible activity of stem cell-derived EVs on differentiated tumor cells *in vivo*, we isolated renal tumor cells from surgical specimens deriving from 17 RCC patients (summarized in Fig. 2). Cells were characterized for the expression of EPCAM, Cytokeratin and Vimentin, in comparison with the tumor of origin (Figs. 2*a* and 2*b*). Stem cell-derived EVs significantly affected primary tumor cell invasion, whereas no significant activity was present on tumor cell proliferation or apoptosis (Figs. 2*c*–2*f*; >20% apoptosis in 3/17 patients).

HLSC-EV pretreatment induced a delay in tumor onset

We subsequently generated RCC tumors in SCID mice by subcutaneous injection of 1,000 renal CSCs. Recovery of tumor cells after 28 days showed the presence of CD105 positive CSCs in a percentage ranging from 14.9% to 90.1% (mean 63.8 ± 24.7; Supporting Information Fig. S2*a*). CD105 positive, but not CD105 negative cells, were able to generate secondary and tertiary tumors.[6,13] *In vitro* apoptosis analysis of recovered cells exhibited an effect of HLSC-EVs on CD105 positive and not on CD105 negative cells, confirming the selective effect of HLSC-EVs on renal CSCs (Supporting Information Figs. S2*b* and S2*c*). We therefore analyzed the effect of MSC- and HLSC-EVs on the subsequent generation and development of RCC tumors (Fig. 3). CSCs were pretreated or not for 24 hr with 50×10^3 MSC-EVs or HLSC-EVs/target cells, the highest effective dose in the *in vitro* experiments. As shown in Figure 3, pretreatment with both MSC-EVs and HLSC-EVs delayed tumor onset of about 2 weeks (Fig. 3*a*). At sacrifice, however, no difference was observed in tumor size among the groups (Fig. 3*b*). In addition, MSC-EV and HLSC-EV pretreatment did not reduce angiogenesis *in vivo* (Fig. 3*c*).

Labeled EV biodistribution in CSCs tumors

In order to assess the EV tumor targeting *in vivo*, DiD labeled EVs were injected in animals with established tumors. By Optical Imaging, using IVIS technology, the fluorescence signals of labeled EVs were detected in all tumors as soon as 5 hr after administration (Figs. 3*d* and 3*e*). Intraperitoneal and intravenous injections were compared to identify the best route of administration for further *in vivo* experiments. For both types of EVs (MSC-EVs and HLSC-EVs), intravenous administration was the best option in which EVs show the maximum accumulation within tumors. Localization reached the pick after 24 hr; then the fluorescent signal started decreasing (Fig. 3*e*). Using intraperitoneal injection, the accumulation of labeled EVs within tumors was significantly lower for both types of EVs (Fig. 3*e*).

HLSC-EV systemic administration reduced tumor growth *in vivo*

On the base of the above results on biodistribution, we studied the effect of MSC-EVs and HLSC-EVs on tumor growth using the intravenous route of administration (i.v.). EVs (1×10^{10}) were administered when subcutaneous tumors were palpable (10 days), twice a week for 4 weeks. As shown in Figure 4, i.v. treatment with HLSC-EVs, but not MSC-EVs, induced a significant reduction of tumor growth. The antitumor effect of HLSC-EVs was statistically significant already starting from

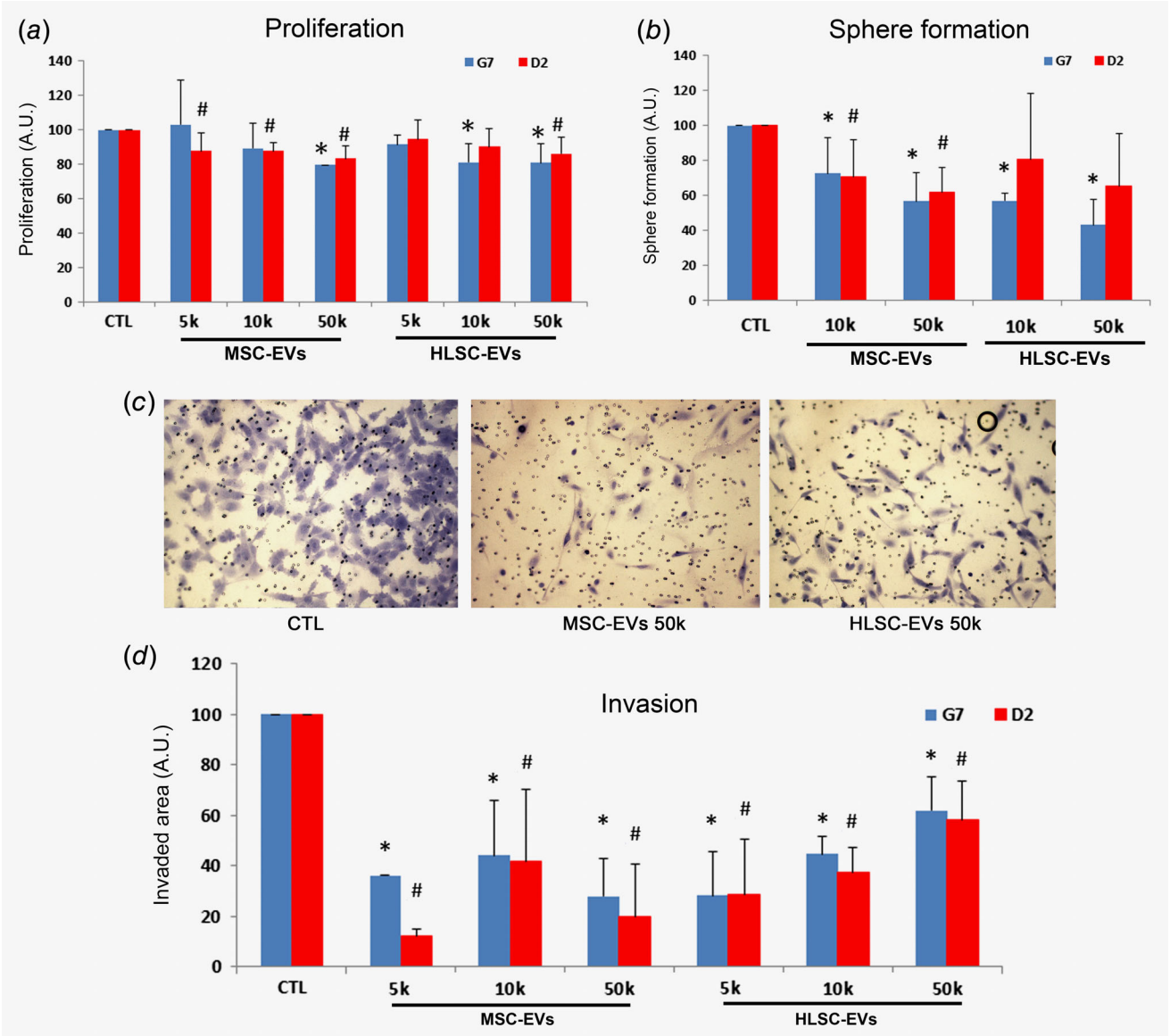

Figure 1. *In vitro* effect of EVs on renal CSCs. (*a*) Proliferation levels, expressed as percentage, of two different renal CSCs clones (G7 and D2) incubated with different doses (ranging from 5 (5k) to 50 (50k) × 10^3 EVs/target cells) of MSC- or HLSC-EVs. (*b*) Quantification of sphere formation ability of renal CSCs stimulated with two different doses of MSC- and HLSC-EVs (10k and 50k EVs/target cell). (*c*) Representative micrographs showing the reduction of renal CSCs invasion capacity induced by MSC- and HLSC-EVs treatment (50k/target cell). Original magnification: 200×. (*d*) Quantification of EVs effect (5, 10 and 50k EVs/target cell) on renal CSCs invasion, represented as percentage of invaded area. Data (*a*, *b* and *c*) are expressed as mean ± SD of three different experiments, normalized to untreated renal CSCs (CTL). $^{*\#}p < 0.05$ *vs*. CTL.

Week 2 of treatment (Fig. 4*a*). Tumor size analysis after mice sacrifice confirmed the tumor reduction exerted by HLSC-EVs observed during the time of treatment (Fig. 4*b*). Moreover, angiogenesis evaluation within tumors revealed a significant reduction in red blood containing vessels in mice treated with HLSC-EVs, but not MSC-EVs (Fig. 4*c*). This is consistent with the antiangiogenic effect of HLSC-EVs but not MSC-EVs on renal human tumor endothelial cells.[12] Moreover, immunohistochemistry for the detection of apoptosis, performed by Tunel assay, showed a significant increase of apoptotic cells in tumors of mice treated with HLSC-EVs but not MSC-EVs (Fig. 4*d*).

HLSC-EV treatment decreased the hematogenous spread to the lungs

In order to evaluate the role of HLSC-EVs in hematogenous CSCs spread to the lungs, we i.v. injected in SCID mice a stable luciferase-expressing renal CSCs clone and luciferase activity

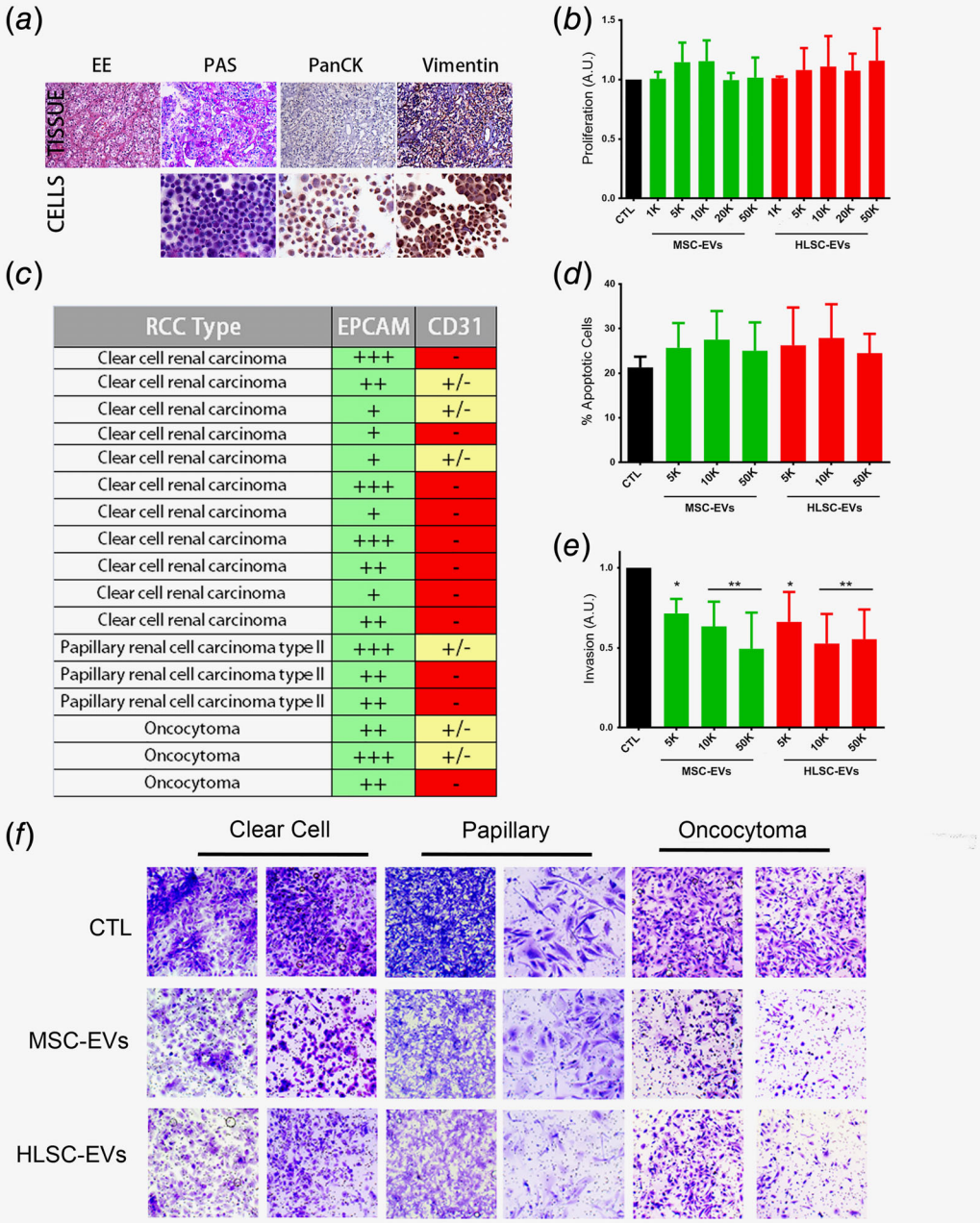

RCC Type	EPCAM	CD31
Clear cell renal carcinoma	+++	-
Clear cell renal carcinoma	++	+/-
Clear cell renal carcinoma	+	+/-
Clear cell renal carcinoma	+	-
Clear cell renal carcinoma	+	+/-
Clear cell renal carcinoma	+++	-
Clear cell renal carcinoma	+	-
Clear cell renal carcinoma	+++	-
Clear cell renal carcinoma	++	-
Clear cell renal carcinoma	+	-
Clear cell renal carcinoma	++	-
Papillary renal cell carcinoma type II	+++	+/-
Papillary renal cell carcinoma type II	++	-
Papillary renal cell carcinoma type II	++	-
Oncocytoma	++	+/-
Oncocytoma	+++	+/-
Oncocytoma	++	-

Figure 2. Effect of MSC- and HLSC-EVs on differentiated RCC cells. (*a*) Representative micrographs showing hematoxylin and eosin (EE) and Periodic Acid Schiff (PAS) staining, and immunohistochemistry for Pan Cytokeratin (PanCK) and Vimentin of the isolated cells (CELLS) compared to the tissue of origin (TISSUE). (*b*) Summary of the different RCC types used for cell isolation, and expression of the epithelial marker EPCAM and of the endothelial marker CD31 evaluated by cytofluorimetric analysis (Score: +++ = ›90%; ++ = ›60%; + = ›30%; +/− = ‹10% positive cells; − = No detected expression). (*c–e*) Quantification of proliferation (C), apoptosis (D) and invasion (E) of RCC-derived cells treated or not with different doses of EVs (1–50k = 1–50 × 10^3 EVs/target cell). Data are represented as mean ± SD of at least two experiments performed at least on two RCC/type, normalized to untreated cells (CTL). *p ‹ 0.05 and **p ‹ 0.001 *vs*. CTL. (*f*) Representative micrographs of invasion assay performed on two RCC/type. Original magnification: 200×.

was analyzed by Optical Imaging in order to monitor tumor progression. Tumor colonies in lungs were detectable after 10 days (Fig. 4*e*). EVs were therefore administered from Day 10, twice a week for 4 weeks. The incidence of lung tumor colonies was analyzed by IVIS. We calculated the lung tumor-free survival with the Kaplan–Maier curve and the result, representing all mice, showed a higher percentage of mice that did not develop detectable CSCs colonies in the HLSC-EVs group

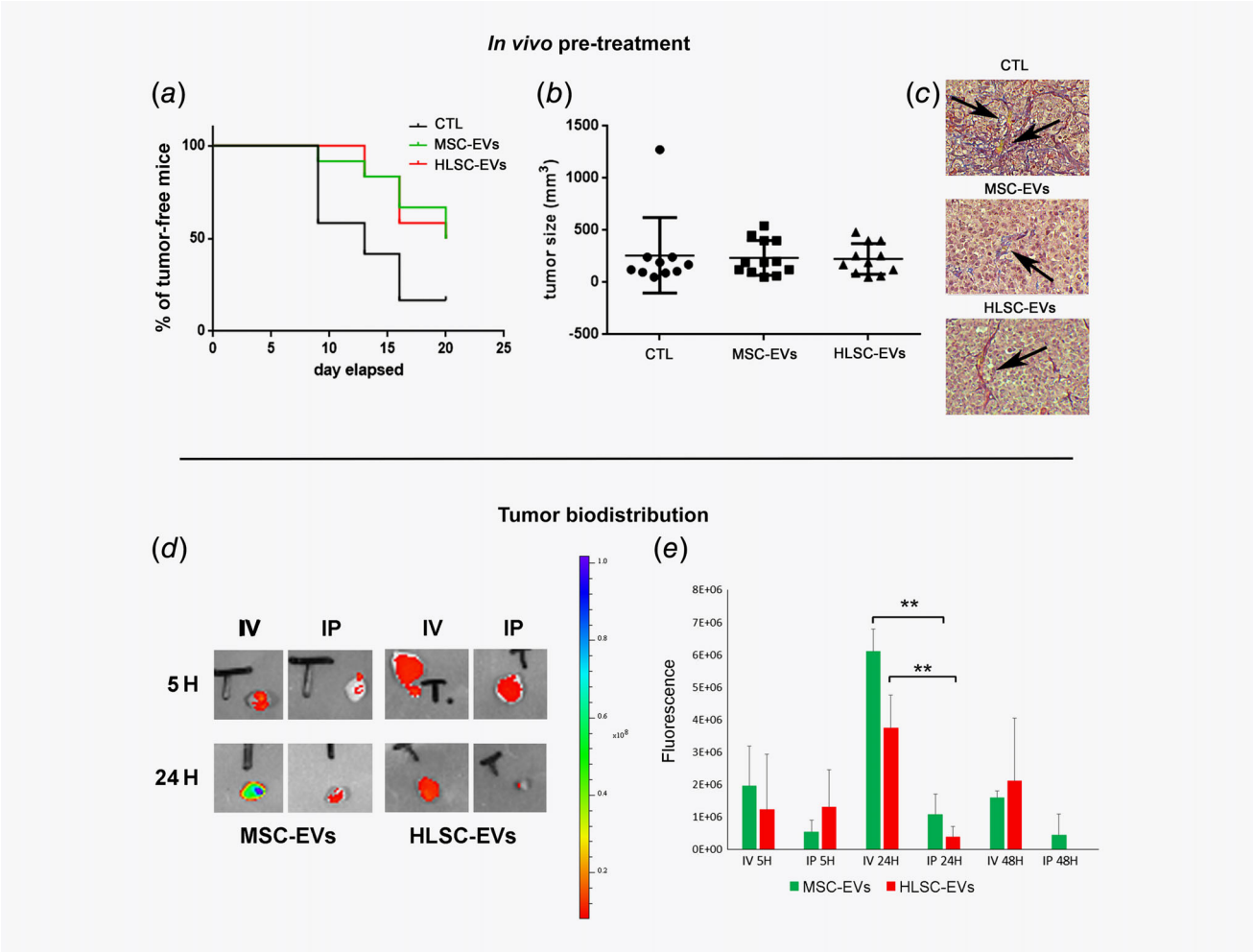

Figure 3. *In vivo* tumor growth after CSCs pretreatment with EVs and EV tumor targeting. (*a*) Percentage of mice that did not develop tumor after subcutaneous injection of renal CSCs pretreated with MSC- or HLSC-EVs, calculated with Kaplan–Meier curve. Data are expressed as mean ± SD of 12 tumors for each group (CTL, MSC-EVs and HLSC-EVs). (*b*) Graph showing tumor size (mm^3) of recovered plugs. (*c*) Representative images of tumors stained with Masson's trichromic reaction. (*d*) Representative images by Optical Imaging of tumors collected at 5 and 24 hr post-EV injection. IV: intravenous, IP: intraperitoneal. (*e*) Fluorescence intensity of dissected tumors measured as Average Radiance ± SD at 5, 24 and 48 hr of mice treated with MSC-EVs and HLSC-EVs. Background signal derived from tumors of untreated mouse ($n = 3$) was subtracted; $^{**}p < 0.01$ intravenous *versus* intraperitoneal injection.

compared to the control group. At Week 3, about 51% of HLSC-EV treated mice did not develop lung tumor foci with respect to 15% of control mice (Figs. 4*f* and 4*g*).

HLSC-EV treatment induced the expression of antitumor miRNAs

To understand if the antitumor effect observed after HLSC-EVs treatment of renal CSCs tumors *in vivo* could be ascribed to antitumor miRNAs carried or induced by EVs, we analyzed the expression of a panel of antitumor miRNAs, known to be downregulated in RCC,[26] on renal CSCs-derived tumors i.v. treated with PBS (CTL), MSC- or HLSC-EVs twice a week for 4 weeks (Fig. 5). Interestingly, in renal CSCs-derived tumors treated i.v. with HLSC-EVs, but not with MSC-EVs, we observed a significant upregulation of the antitumor miRNAs miR-Let7b, miR-200b, miR-200c and miR-223, and a slight increase of miR-145 (Fig. 5*a*), confirming the effect on tumor growth inhibition of HLSC-EVs, but not of MSC-EVs, observed *in vivo*.

In parallel, we evaluated the expression of some targets of the induced miRNAs, such as C-MYC (miR-145 target), EGFR (miR-145 target), ZEB1 and ZEB2 (miR-200b and miR-200c targets), and MMP1 (miR-145 and miR-200b target; Fig. 5*b*). EGFR, ZEB2 and MMP1 were found downregulated in HLSC-EVs treated tumors.

We also confirmed that these microRNAs are expressed at low level in renal CSCs (Supporting Information Figs. S3*a* and S3*b*). Indeed, the antitumor miRNAs were present at

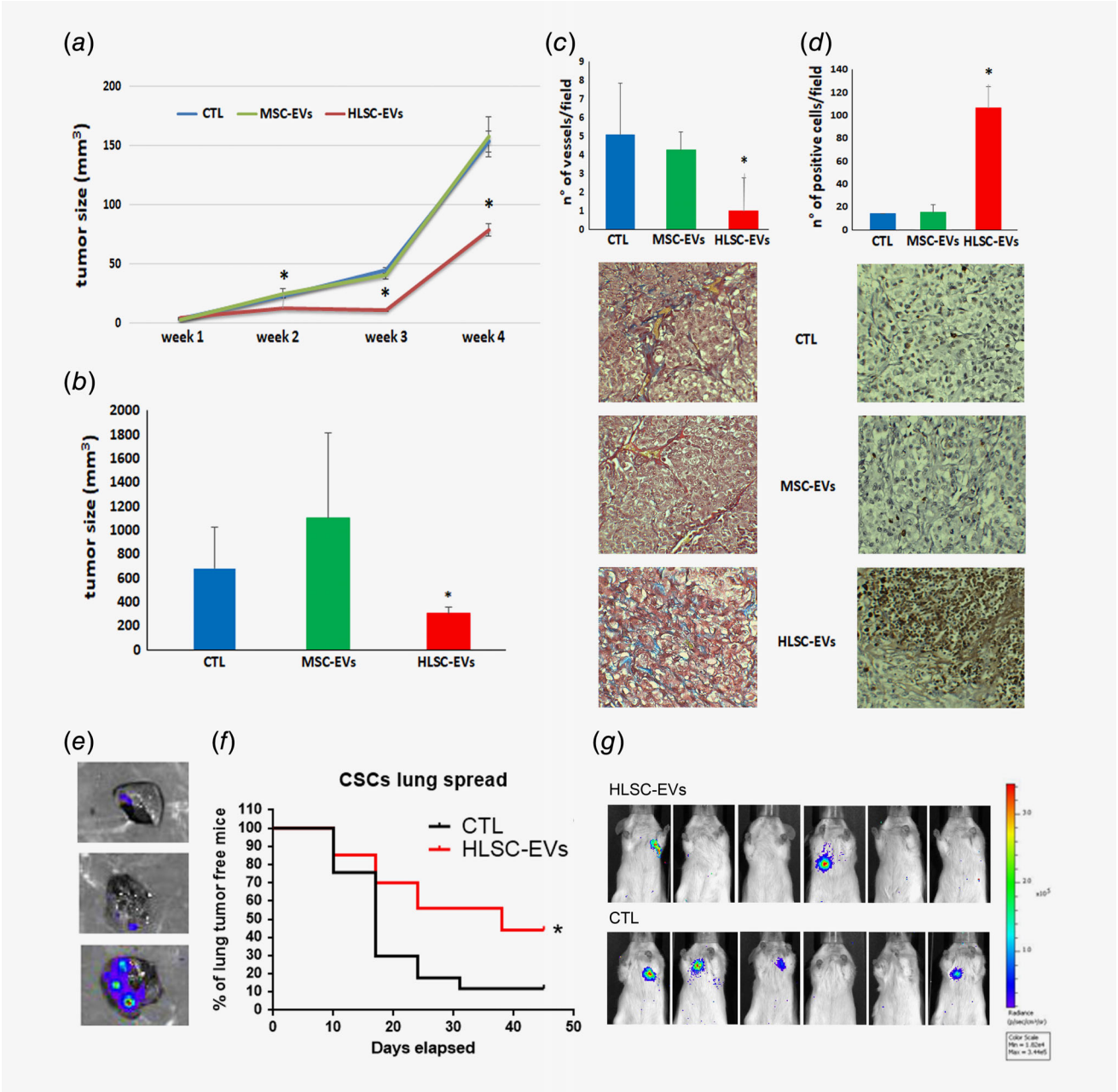

Figure 4. Intravenous injection of HLSC-EVs reduced tumor growth and delayed CSCs lung spread. (*a*) Tumor size (mm^3) of untreated mice (CTL), and of mice i.v. treated with MSC- or HLSC-EVs during the experiment. (*b*) Tumor size (mm^3) of recovered plugs after sacrifice. (*c*) Evaluation of angiogenesis within plugs, expressed as number of vessels connected to mouse vasculature/field, and representative images of vessels stained with Masson's trichromic reaction. (*d*) Tumor apoptosis evaluation by Tunel assay, expressed as number of TUNEL positive cells/field, and representative micrographs showing apoptosis within tumors. (*a–d*) Data are expressed as mean ± SEM of $n = 20$ tumors for control group (CTL), $n = 18$ for HLSC-EVs group and $n = 14$ for MSC-EVs group. *$p > 0.05$ *vs*. CTL. (*e*) Representative micrographs showing IVIS analysis of lung CSCs foci after 10 days from i.v. injection of renal CSCs; (*f*) Kaplan–Meier curve showing the percentage of mice that did not develop lung tumors during the time of experiment. Data are expressed as mean ± SEM of 24 HLSC-EVs and 24 PBS treated mice. *$p = 0.0016$. (*g*) Representative micrographs showing IVIS analysis of lungs at Week 3.

different levels in HLSC-EVs (Supporting Information Fig. S3*c*). In particular, among the antitumor miRNAs induced *in vivo* by HLSC-EV treatment, miR-145 and miR-Let7b are present at high levels (CT < 30), while low levels of miR-200b, miR-200c and miR-223 were detected in HLSC-EVs (Supporting Information Fig. S3*c*). In order to evaluate whether these miRNAs were transferred or induced by EV treatment, we blocked cell transcription with α-Amanitin, as

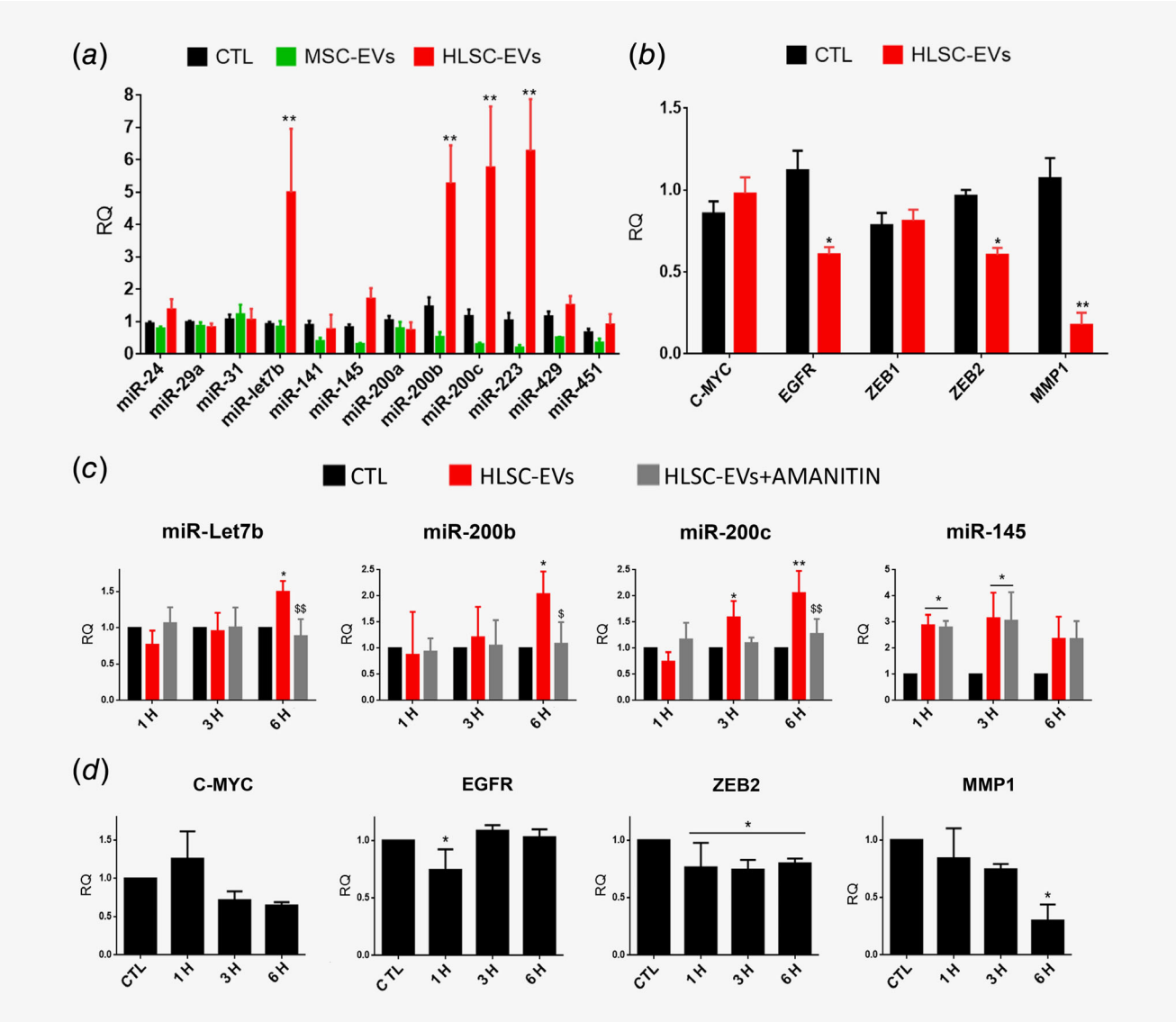

Figure 5. HLSC-EVs induce antitumor miRNA expression both *in vivo* and *in vitro*. (*a*) Antitumor miRNAs expression on renal CSCs-derived tumors, evaluated by real-time PCR, after 4 weeks of EV-treatment. Data are expressed as mean ± SD of Relative Quantification (RQ) normalized to PBS-treated tumors (CTL) and to RNU6B of 10 CTL, 10 MSC- and 10 HLSC-EV treated tumors. $^{**}p < 0.001$ *vs*. CTL. (*b*) Real-time PCR analysis of antitumor miRNA targets in renal CSC-derived tumors i.v. treated for 4 weeks with HLSC-EVs ($n = 10$). Data are expressed as mean ± SD of Relative Quantification (RQ) normalized to PBS-treated tumors (CTL) and to TBP. $^{**}p < 0.001$ *vs*. CTL. (*c* and *d*) Real-time PCR analysis of renal CSCs treated with HLSC-EVs alone or in the presence of α-Amanitin for 1, 3 and 6 hr, showing the expression of miR-Let7b, miR200b, miR-200c and miR-145 (*c*) and of their targets C-MYC, EGFR, ZEB2 and MMP1 (*d*). Data (*c* and *d*) are expressed as Relative Quantification (RQ) of three different experiments, normalized to RNU6B or TBP and to untreated cells (CTL). $^{*}p < 0.05$ and $^{**}p < 0.001$ *vs*. CTL; $^{\$}p < 0.05$ and $^{\$\$}p < 0.05$ *vs*. HLSC-EVs.

previously described,[11] and miRNA expression in renal CSCs *in vitro* at different time points was evaluated. As shown in Figure 5*c*, α-Amanitin abrogated the increase of miR-Let7b, miR-200c and miR-200b induced by HLSC-EV treatment, thus suggesting an EV mediated upregulation. On the contrary, renal CSCs treated with HLSC-EVs showed an early increase of miR-145 levels, also in the presence of α-Amanitin, suggesting a direct transfer of this miRNA. As a result of both miR-transfer and induction, we observed a significant downregulation *in vitro* of the specific targets EGFR, ZEB2, and MMP1 (Fig. 5*d*), thus confirming our *in vivo* results.

In vitro antiproliferative, antiinvasive and proapoptotic effect of antitumor miRNAs induced by HLSC-EVs

Finally, we analyzed the role of the identified antitumor miRNAs induced by HLSC-EV treatment both *in vitro* and *in vivo*, by transfecting renal CSCs with mimics for the panel of antitumor miRNAs tested in the *in vivo* experiments. Transfection efficacy is

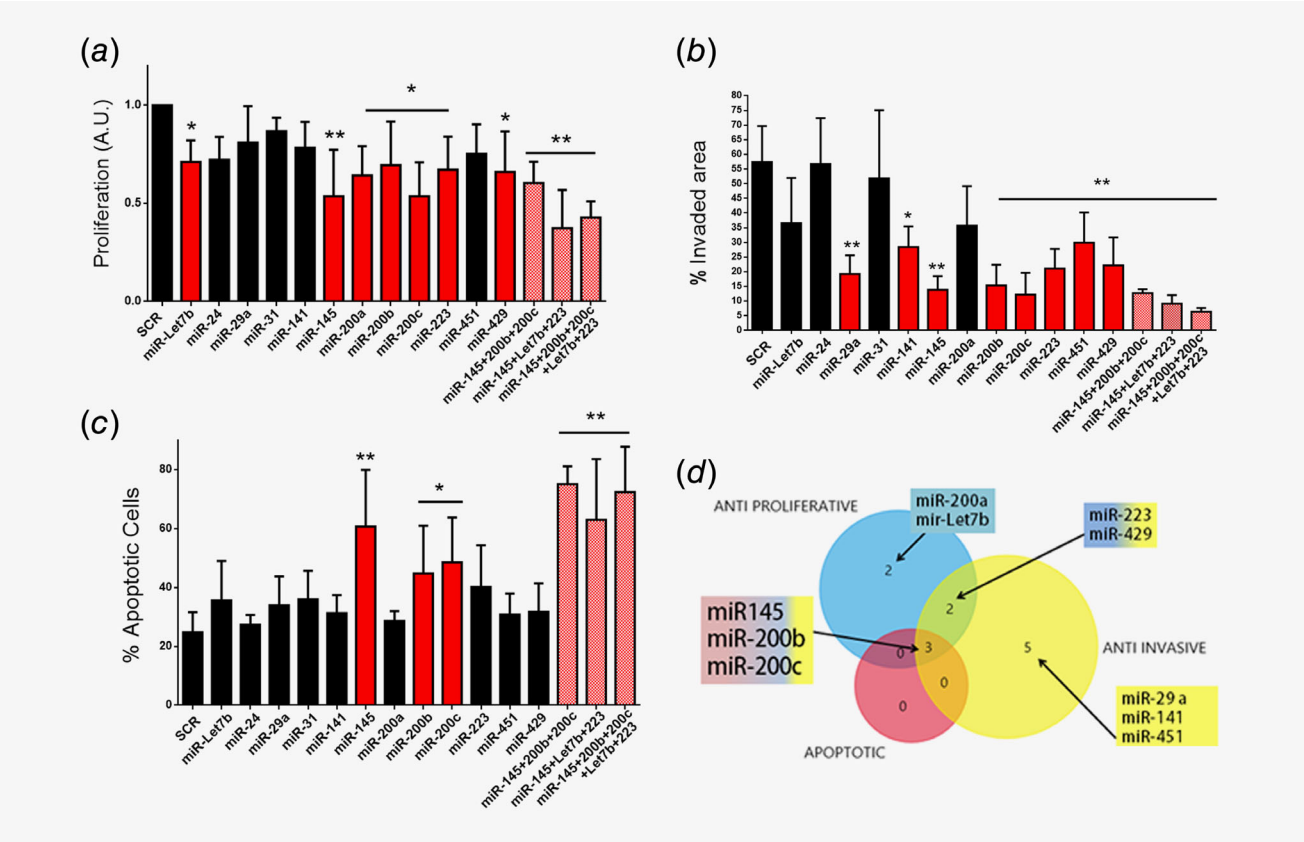

Figure 6. Transfection of renal CSCs with antitumor miRNAs. (*a–c*) Functional assays performed on transfected renal CSCs, showing the effect of selected mimics on proliferation (*a*), apoptosis (*b*) and invasion (*c*) 72 hr after transfection. Data are expressed as mean ± SD of three independent experiments. *$p < 0.05$ and **$p < 0.001$ *vs*. CSCs transfection with scrambled sequences (SCR). (*d*) Schematic representation of the functional effect of specific mimics.

shown in Supporting Information Figure 3*d*. Transfection of renal CSCs with mimics for miR-Let7b, miR-145, miR-200a, miR-200b, miR-200c, miR-223 and miR-429 (red bars, Figs. 6*a*–6*c*) resulted in a significant reduction of renal CSCs proliferative ability (Fig. 6*a*). A significant induction of apoptosis was observed when renal CSCs were transfected with mimics for miR-145, miR-200b and miR-200c (Fig. 6*b*). In addition, we demonstrated a significant anti-invasive effect of CSCs transfection with mimics for miR-29a, miR-141, miR-145, miR-200b, miR-200c, miR-223, miR-451 and miR-429 (Fig. 6*c*).

Co-transfection of CSCs with miR-145, that was directly transferred by HLSC-EVs to CSCs, together with miR-200b and miR-200c or with miR-Let7b and miR-223, whose expression in CSCs was induced by HLSC-EVs treatment (Fig. 5), resulted in a higher effect in respect with the single miR transfection on proliferation, apoptosis and invasion (Figs. 6*a* and 6*c*).

We therefore demonstrated the anti-invasive, antiproliferative and proapoptotic effects of selected miRNAs (Fig. 6*d*). Moreover, three miRNAs showed antiproliferative, anti-invasive and apoptotic activity: miR-145, miR-200b and miR-200c. Interestingly, these three miRNAs are those induced by HLSC-EVs treatment of renal CSCs-derived tumors *in vivo* (Fig. 5*a*).

Discussion

In the present paper, we demonstrate that intravenous administration of EVs derived from a liver resident population of mesenchymal stromal cells reduced development, growth and improved lung tumor-free survival of a RCC obtained by injection of renal CSCs. This effect was not shared by EVs derived from bone marrow MSC. HLSC-EVs targeted the tumor and induced transfer and upregulation of selected antitumor microRNAs, able to affect CSC growth, invasion and survival. Stem cell-derived EVs, and in particular MSC-EVs, acquire increasing interest for their effect on tissue repair, limiting inflammation and promoting restoration of injured tissue.[21] The role of stem cell-derived EVs on *in vivo* tumor growth and progression is however debated, and appears related to EV origin, to the tumor nature as well as to the modality of EV treatment.[27–31] For instance, tumor cell pretreatment with EVs from embryonic stem cells inhibited breast and colorectal carcinoma development.[28] Similarly, Wharton Jelly MSC-EVs inhibited bladder carcinoma when mixed with cells before their *in vivo* implantation.[29] The same Wharton Jelly MSC-EVs showed an opposite effect when tested on renal carcinoma xenografts, increasing its

development.[30] Data on bone marrow MSC-EVs are quite contradictory as well.[27] Indeed, pretreatment with bone marrow MSCs limited myeloma growth and promoted dormancy of breast tumors,[32,33] and subcutaneous injection of MSC-EVs limited breast tumor angiogenesis.[34] Moreover, intratumor injection of bone marrow MSC-EVs limited tumor growth of ovarian, hepatocellular carcinoma and Kaposi's sarcoma.[35] We also confirmed here that pretreatment of renal carcinomas with bone marrow MSC-EVs delayed tumor formation, although no difference was observed when tumor started to grow exponentially. On the other side, pretreatment with bone marrow MSC-EVs promoted myeloma, breast, gastric and colon tumor growth and angiogenesis.[36–39] Similarly, pretreatment with human umbilical cord MSC-EVs increased the growth of lung adenocarcinoma.[40] In the present paper, we tested for the first time the use of stem cell-EVs in a systemic intravenous administration on tumor growth. The results showed the inefficacy of MSC-EV intravenous administration whereas HLSC-EVs showed a consistent effect on CSC tumor growth and lung tumor spread. The antitumor ability of EVs from another source of tissue-resident stem cells, that is cardiac stem cells, was recently reported using an intraperitoneal administration.[41] HLSC-EVs therefore appear an interesting source of EVs with antitumor characteristics. HLSC-EVs were previously reported to inhibit liver carcinomas after intratumor injection, and to induce apoptosis of renal CSCs.[13,17] In this article, besides confirming the proapoptotic effects of HLSC-EVs, we also found an effect on CSC invasion and organization into spheres, a stem-related characteristic. At variance, the effect of HLSC-EVs on differentiated primary tumor cell lines isolated from renal carcinomas was restricted to inhibition of invasion. This is different from the data obtained *in vivo* showing the proapoptotic effect of HLSC-EVs on the majority of cells of the tumor rather than on a selected stem-related cell population. It can be therefore speculated that the observed *in vivo* effect could be dependent on a combined action on the tumor cells as well as on the tumor endothelium, confirmed by the reduction of angiogenesis. Indeed, the effect of HLSC-EVs on renal tumor endothelial cells has been recently detailed.[11] The systemic administration of EVs led to a rapid intratumor localization, as soon as 5 hr. This was higher than that obtained with intraperitoneal injection, and could be related to the increased permeability of tumor vessels and to intrinsic targeting characteristics. EVs possess unique features in terms of targeting and natural cargo/drug delivering. In fact, EVs, compared to synthetic liposomes, display an excellent biological tolerance due to their endogenous nature and an intrinsic ability to cross over cellular and tissue barriers.[42] Moreover, different types of EVs show enhanced localization in specific tissues, and may be used as selective delivery system.[43] Furthermore, thanks to the presence of adhesion surface molecules, EVs have the advantage of rapid internalization.[7] The uptake of HLSC-EVs by tumor cells is also shown by the increase of miR-145, which is highly expressed by HLSC-EVs. In addition, other antitumor miRNAs were interestingly upregulated in EV treated tumors. This appears related to induction of miRNAs by HLSC, as the EVs themselves did not show high level of these miRNAs in their cargo. Moreover, *in vitro* experiments using α-Amanitin to inhibit *de novo* transcription clearly confirmed the rapid upregulation of miR-145, but not of miR-200 family, indicating the absence of transfer from EVs. MiR-145 is a well-known antitumor miRNA, downregulated in many solid tumors, and it is involved in many steps of tumorigenesis. In particular, miR-145 modulates oncogenes involved in proliferation, angiogenesis, CSCs differentiation and invasion.[44] The antitumor effect of miR-145 in RCC mainly involves the regulation of genes orchestrating cell invasion.[45–47] Interestingly, renal CSCs transfection with a panel of antitumor miRNAs confirmed in our model that miR-145 was active in blocking CSCs invasion, proliferation and survival. Moreover, in renal CSCs treated with HLSC-EVs, we observed both *in vitro* and *in vivo* the downregulation of EGFR and MMP1, described as direct miR-145 targets.[48,49] In addition, HLSC-EVs induced the transcription of miR-200b and miR-200c, members of the miR-200 family, known to be downregulated in RCC.[50] Likewise, we observed that transfection of renal CSCs with miR-200b and miR-200c impaired renal CSCs functions. HLSC-EVs not only increased miR-200 family but also reduced their specific target ZEB2, one of the main regulators of epithelial–mesenchymal transition. However, it cannot be excluded that other molecular mechanisms may be involved in the complex setting of the *in vivo* tumor growth. In particular, other EV cargo, such as proteins, lipids or RNA species as well as modulation of other cell functions, such as activation of signal transduction, or effects on cell metabolism, could play a role in the observed antitumor effects on renal CSCs.

In conclusion, our results showed a specific antitumor effect of HLSC-EVs, and not of MSC-EVs, on CSC-derived renal tumors *in vivo*, that could be ascribed to the transfer and induction of specific antitumor miRNAs. Our study provides further evidence on the clinical use of HLSC-EVs in renal tumor treatment, by their possible administration alone or in combination with the current therapies.

Acknowledgements

The authors thank Federica Antico for the histological assistance and Unicyte AG for providing HLSC. Our study was supported by Associazione Italiana per la Ricerca sul Cancro (A.I.R.C.), project IG2015 16,973 and by grant no. 071215 from Unicyte to GC and BB.

Conflict of interest

V.F. and G.C. are inventors in a related patent application. G.C. is a member of the scientific advisory board of Unicyte AG.

References

1. Znaor A, Lortet-Tieulent J, Laversanne M, et al. International variations and trends in renal cell carcinoma incidence and mortality. *Eur Urol* 2015;67:519–30.
2. Williamson SR, Taneja K, Cheng L. Renal cell carcinoma staging: pitfalls, challenges, and updates. *Histopathology* 2019;74:18–30.
3. Makhov P, Joshi S, Ghatalia P, et al. Resistance to systemic therapies in clear cell renal cell carcinoma: mechanisms and management strategies. *Mol Cancer Ther* 2018;17: 1355–64.
4. Cabarcas SM, Mathews LA, Farrar WL. The cancer stem cell niche—there goes the neighborhood? *Int J Cancer* 2011;129:2315–27.
5. Bussolati B, Dekel B, Azzarone B, et al. Human renal cancer stem cells. *Cancer Lett* 2013;338: 141–6.
6. Bussolati B, Bruno S, Grange C, et al. Identification of a tumor-initiating stem cell population in human renal carcinomas. *FASEB J* 2008;22:3696–705.
7. Camussi G, Deregibus MC, Bruno S, et al. Exosome/microvesicle-mediated epigenetic reprogramming of cells. *Am J Cancer Res* 2011;1:98–110.
8. Raposo G, Stoorvogel W. Extracellular vesicles: exosomes, microvesicles, and friends. *J Cell Biol* 2013;200:373–83.
9. Turturici G, Tinnirello R, Sconzo G, et al. Extracellular membrane vesicles as a mechanism of cell-to-cell communication: advantages and disadvantages. *Am J Physiol Cell Physiol* 2014;306: C621–33.
10. Brossa A, Fonsato V, Bussolati B. Anti-tumor activity of stem cell-derived extracellular vesicles. *Oncotarget* 2019;10:1872–3.
11. Lopatina T, Grange C, Fonsato V, et al. Extracellular vesicles from human liver stem cells inhibit tumor angiogenesis. *Int J Cancer* 2019;144:322–33.
12. Grange C, Tritta S, Tapparo M, et al. Stem cell-derived extracellular vesicles inhibit and revert fibrosis progression in a mouse model of diabetic nephropathy. *Sci Rep* 2019;9:4468.
13. Fonsato V, De Lena M, Tritta S, et al. Human liver stem cell-derived extracellular vesicles enhance cancer stem cell sensitivity to tyrosine kinase inhibitors through Akt/mTOR/PTEN combined modulation. *Oncotarget* 2018;9:36151–65.
14. Brossa A, Buono L, Bussolati B. Effect of the monoclonal antibody TRC105 in combination with Sunitinib on renal tumor derived endothelial cells. *Oncotarget* 2018;9:22680–92.
15. Herrera MB, Bruno S, Buttiglieri S, et al. Isolation and characterization of a stem cell population from adult human liver. *Stem Cells* 2006;24:2840–50.
16. Fonsato V, Herrera MB, Buttiglieri S, et al. Use of a rotary bioartificial liver in the differentiation of human liver stem cells. *Tissue Eng Part C Methods* 2010;16:123–32.
17. Fonsato V, Collino F, Herrera MB, et al. Human liver stem cell-derived microvesicles inhibit hepatoma growth in SCID mice by delivering antitumor microRNAs. *Stem Cells* 2012;30:1985–98.
18. Herrera Sanchez MB, Previdi S, Bruno S, et al. Extracellular vesicles from human liver stem cells restore argininosuccinate synthase deficiency. *Stem Cell Res Ther* 2017;8:176.
19. Grange C, Tapparo M, Bruno S, et al. Biodistribution of mesenchymal stem cell-derived extracellular vesicles in a model of acute kidney injury monitored by optical imaging. *Int J Mol Med* 2014;33:1055–63.
20. Webber J, Clayton A. How pure are your vesicles? *J Extracell Vesicles* 2013;10:2.
21. Bruno S, Tapparo M, Collino F, et al. Renal regenerative potential of different extracellular vesicle populations derived from bone marrow mesenchymal stromal cells. *Tissue Eng Part A* 2017;23: 1262–73.
22. Grange C, Tapparo M, Collino F, et al. Microvesicles released from human renal cancer stem cells stimulate angiogenesis and formation of lung premetastatic niche. *Cancer Res* 2011;71:5346–56.
23. Brossa A, Papadimitriou E, Collino F, et al. Role of CD133 molecule in Wnt response and renal repair. *Stem Cells Transl Med* 2018;7:283–94.
24. Jin C, Fotaki G, Ramachandran M, et al. Safe engineering of CAR T cells for adoptive cell therapy of cancer using long-term episomal gene transfer. *EMBO Mol Med* 2016;8:702–11.
25. D'Amico L, Patanè S, Grange C, et al. Primary breast cancer stem-like cells metastasise to bone, switch phenotype and acquire a bone tropism signature. *Br J Cancer* 2013;108:2525–36.
26. Grange C, Collino F, Tapparo M, et al. Oncogenic micro-RNAs and renal cell carcinoma. *Front Oncol* 2014;4:49.
27. Vakhshiteh F, Atyabi F, Ostad SN. Mesenchymal stem cell exosomes: a two-edged sword in cancer therapy. *Int J Nanomedicine* 2019;14:2847–59.
28. Zhou S, Abdouh M, Arena V, et al. Reprogramming malignant cancer cells toward a benign phenotype following exposure to human embryonic stem cell microenvironment. *PLoS One* 2017; 12:e0169899.
29. Wu S, Ju GQ, Du T, et al. Microvesicles derived from human umbilical cord Wharton's jelly mesenchymal stem cells attenuate bladder tumor cell growth in vitro and in vivo. *PLoS One* 2013;8: e61366.
30. Du T, Ju G, Wu S, et al. Microvesicles derived from human Wharton's jelly mesenchymal stem cells promote human renal cancer cell growth and aggressiveness through induction of hepatocyte growth factor. *PLoS One* 2014;9:e96836.
31. Peak TC, Praharaj PP, Panigrahi GK, et al. Exosomes secreted by placental stem cells selectively inhibit growth of aggressive prostate cancer cells. *Biochem Biophys Res Commun* 2018;499: 1004–10.
32. Roccaro AM, Sacco A, Maiso P, et al. BM mesenchymal stromal cell-derived exosomes facilitate multiple myeloma progression. *J Clin Invest* 2013; 123:1542–55.
33. Ono M, Kosaka N, Tominaga N, et al. Exosomes from bone marrow mesenchymal stem cells contain a microRNA that promotes dormancy in metastatic breast cancer cells. *Sci Signal* 2014;7: ra63.
34. Lee JK, Park SR, Jung BK, et al. Exosomes derived from mesenchymal stem cells suppress angiogenesis by down-regulating VEGF expression in breast cancer cells. *PLoS One* 2013;8:e84256.
35. Bruno S, Collino F, Deregibus MC, et al. Microvesicles derived from human bone marrow mesenchymal stem cells inhibit tumor growth. *Stem Cells Dev* 2013;22:758–71.
36. Zhou X, Li T, Chen Y, et al. Mesenchymal stem cell-derived extracellular vesicles promote the in vitro proliferation and migration of breast cancer cells through the activation of the ERK pathway. *Int J Oncol* 2019;54:1843–52.
37. Gu H, Ji R, Zhang X, et al. Exosomes derived from human mesenchymal stem cells promote gastric cancer cell growth and migration via the activation of the Akt pathway. *Mol Med Rep* 2016; 14:3452–8.
38. Ji R, Zhang B, Zhang X, et al. Exosomes derived from human mesenchymal stem cells confer drug resistance in gastric cancer. *Cell Cycle* 2015;14: 2473–83.
39. Zhu W, Huang L, Li Y, et al. Exosomes derived from human bone marrow mesenchymal stem cells promote tumor growth in vivo. *Cancer Lett* 2012;315:28–37.
40. Dong L, Pu Y, Zhang L, et al. Human umbilical cord mesenchymal stem cell-derived extracellular vesicles promote lung adenocarcinoma growth by transferring miR-410. *Cell Death Dis* 2018;9:218.
41. Grigorian-Shamagian L, Fereydooni S, Liu W, et al. Harnessing the heart's resistance to malignant tumors: cardiac-derived extracellular vesicles decrease fibrosarcoma growth and leukemia-related mortality in rodents. *Oncotarget* 2017;8: 99624–36.
42. Murphy DE, de Jong OG, Brouwer M, et al. Extracellular vesicle-based therapeutics: natural versus engineered targeting and trafficking. *Exp Mol Med* 2019;51:32.
43. Kooijmans SAA, Schiffelers RM, Zarovni N, et al. Modulation of tissue tropism and biological activity of exosomes and other extracellular vesicles: new nanotools for cancer treatment. *Pharmacol Res* 2016;111:487–500.
44. Cui SY, Wang R, Chen LB. MicroRNA-145: a potent tumour suppressor that regulates multiple cellular pathways. *J Cell Mol Med* 2014;18: 1913–26.
45. Wu D, Li M, Wang L, et al. microRNA-145 inhibits cell proliferation, migration and invasion by targeting matrix metallopeptidase-11 in renal cell carcinoma. *Mol Med Rep* 2014;10:393–8.
46. Doberstein K, Steinmeyer N, Hartmetz AK, et al. MicroRNA-145 targets the metalloprotease ADAM17 and is suppressed in renal cell carcinoma patients. *Neoplasia* 2013;15:218–30.
47. Lu R, Ji Z, Li X, et al. miR-145 functions as tumor suppressor and targets two oncogenes, ANGPT2 and NEDD9, in renal cell carcinoma. *J Cancer Res Clin Oncol* 2014;140:387–97.
48. Lu Y, Chopp M, Zheng X, et al. Overexpression of miR-145 in U87 cells reduces glioma cell malignant phenotype and promotes survival after in vivo implantation. *Int J Oncol* 2015;46:1031–8.
49. Zheng L, Pu J, Qi T, et al. miRNA-145 targets v-ets erythroblastosis virus E26 oncogene homolog 1 to suppress the invasion, metastasis, and angiogenesis of gastric cancer cells. *Mol Cancer Res* 2013;11:182–93.
50. Duns G, van den Berg A, van Dijk MC, et al. The entire miR-200 seed family is strongly deregulated in clear cell renal cell cancer compared to the proximal tubular epithelial cells of the kidney. *Genes Chromosomes Cancer* 2013;52: 165–73.